UAV-aided uplink NOMA based on MEC in IoT networks: Secrecy offloading and Optimization

Anh-Nhat Nguyen, Tung-Son Ngo, Ngoc-Anh Bui, Phuong-Chi Le, and Gia-Huy Nguyen

Department of Computing Fundamentals, FPT University, Hanoi 10000, Vietnam
{nhatna3, sonnt69, anhbn5, chilp2}@fe.edu.vn
huynghe180064@fpt.edu.vn

Abstract. This paper studied unmanned aerial vehicle (UAV)-aided uplink nonorthogonal multiple access (NOMA)-based mobile-edge computing (MEC) in Internet of Things (IoT) systems. Specifically, two resource-constrained edge device (ED) clusters want to offload their tasks for a UAV equipped with a MEC server in the presence of a passive eavesdropper. We derive the expression of secrecy successful computation probability (SSCP) for the system to evaluate its secrecy performance. In addition, we present an optimization problem formulation that optimizes the SSCP by establishing optimal values for UAV's location and altitude. An approach based on particle swarm optimization (PSO) was used to solve the problem. The precision of our study conducted with diverse parameters, involving the average transmit signal-to-noise ratio (SNR), the number of EDs in each cluster, and the location and altitude of the UAV, was finally confirmed by the Monte Carlo simulation results.

Keywords: internet of things · unmanned aerial vehicles · nonorthogonal multiple access · mobile edge computing · physical layer security.

1 Introduction

Internet of Things (IoT) mobile data traffic demand has exploded in recent years. However, the energy-constrained, low-computing-capability mobile terminal cannot support a growing number of applications requiring sustainable and intensive computations, such as virtual/augmented reality, remote operations, and autonomous driving [1].

In order to overcome these challenges, mobile-edge computing (MEC) and nonorthogonal multiple access (NOMA) have both been presented as possible approaches for IoT networks [2]. The main idea of MEC is to use the available computing resources around it to let mobile terminals compute, whereas NOMA allows numerous mobile terminals to communicate in the power domain using the same time/frequency resource block. NOMA is distinguished by the requirement for superposition coding at the broadcasting end and successive interference cancellation (SIC) at the receiving end [3]. In general, MEC offers two types of compute offloading modes: partial offloading and binary offloading [4]. In addition, the combination of NOMA and MEC techniques to enhance offloading efficacy has been studied recently [5, 6]. The research presented in [5] studied two distinct NOMA-enabled offloading approaches. An analysis conducted in [6] examined a NOMA-enabled MEC system comprising two edge device (ED) clusters linked through a multi-antenna access point (AP).

However, MEC significantly depends on the transfer and calculations of data between devices and servers. The random distribution EDs often leads to signal reception issues, and EDs' power-limitation heavily limits their transmission range. A feasible way to surpass these deficiencies in wireless communication is to use unmanned aerial vehicle (UAV) [7]. A unique characteristic of UAV is the establishment of Line-of-Sight (LoS) connections between UAV and EDs, permitting UAV to provide signal coverage, preventing small-scale fading and potentially improving network performance [8]. Additionally, the ability of UAVs to maneuver in close proximity to EDs facilitates the deployment of robust communication linkages. Therefore, an UAV can function as a reliable and versatile transport for an edge server [9] or as a relay connecting EDs to a base station (BS) [10].

Moreover, the broadcast nature of wireless transmission renders the tasks offloaded by EDs to the MEC server via wireless channels susceptible to being intercepted by malicious eavesdroppers, leading to information leakage issues. Consequently, evaluating the MEC system's security is crucial. Physical-layer security (PLS) utilizes the inherent characteristics of wireless channels to safeguard communications, and has gathered significant attentions in the wireless communication domain. Nevertheless, complete security remains unattainable because of the transmitter's incapacity to detect the channel state information (CSI) of eavesdroppers and the stringent latency limits imposed by certain systems. In [12], eavesdropper CSI is assumed to be a bounded channel uncertainty model and secure energy efficiency in NOMA-based mMTC networks can be optimized while meeting terminal device delay requirements. In [13], the authors first minimized users' total energy consumption under the constraints of secure offloading rate, computation time, and secrecy outage probability, then minimized it by considering two users' priorities.

Driven by the preceding discourses, this paper investigates the secrecy offloading performance for IoT networks employing UAV-aided NOMA-MEC under Rayleigh fading channels. Additionally, we take into account the probability of LoS and non-LoS (NLoS) for wireless channels between UAV and mobile devices. Moreover, the two best EDs from two device clusters is selected to offload the tasks. Finally, we propose an optimization problem to enhance the secrecy performance of the system. The following are the primary contribution of our paper:

- We propose a UAV-aided NOMA-MEC with passive eavesdropping for IoT networks. In addition, we employ ED selection strategy to enhance secrecy performance of the system.

- We derive closed-form expressions of SSCP for the entire system. In addition, we formulated a problem for maximizing SSCP by optimizing the UAV's location and altitude. The problem was solved using a PSO-based algorithm.
- To confirm the efficacy of our system, numerical results are used to evaluate the system's secrecy performance, including transmit power, number of EDs, and the location and altitude of UAV.

The remaining section of the paper is structured as follows. In Section 2, the communication protocol and system model are introduced. The SSCP and optimization problem are examined in Section 3. In Section 4, numerical results are demonstrated and discussed. Section 5 summarizes the final conclusions.

2 System Model and Communication Protocol

2.1 System and channel model

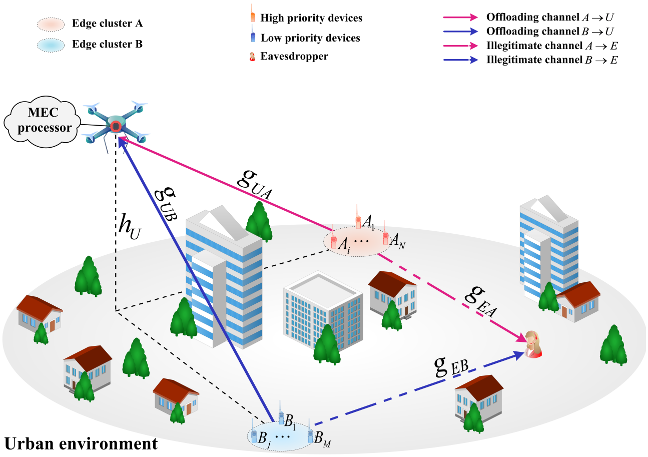

Fig. 1: System model for a UAV NOMA-MEC in IoT network.

As illustrated in Fig. 1, we consider a UAV-aided NOMA-MEC in IoT network in which consists of two edge device clusters A and B, where A is a high-priority device cluster and B is a low-priority cluster, denoted $A_i, (1 \leq i \leq N)$ and $B_j, (1 \leq j \leq M)$, respectively. These two clusters of devices are resource-constrained, so they wish to offload confidential tasks to the UAV, denoted by U, to have U handle the computation in the presence of a passive eavesdropper, denoted by E. All devices are assumed to being equipped with a single antenna operating in half-duplex mode and in urban environments.

Without loss of generality, we utilized a 3D Cartesian coordinate system, we use $U\left(x_U, y_U, h_U\right)$, $A_i\left(x_{A_i}, y_{A_i}, 0\right)$, $B_j\left(x_{B_j}, y_{B_j}, 0\right)$, and $E\left(x_E, y_E, 0\right)$. Assuming the large-scale fading channel of UAV and EDs is governed by a LoS and NLoS probabilistic model. Taking into consideration the probability of LoS and NLoS links between U and EDs, the mean path loss is calculated as follows [14]:

$$\mathfrak{L}_{ab}\left(d_{ab},\varphi_{ab}\right)=\left[\mathfrak{K}_{LoS}+\frac{\mathfrak{K}_{LoS}-\mathfrak{K}_{NLoS}}{1+\mathfrak{B}\exp\left(-\frac{180}{\pi}\mathfrak{A}\varphi_{ab}+\mathfrak{A}\mathfrak{B}\right)}\right]d_{ab}^{\sigma}, \tag{1}$$

where $ab\in\left(UA_i,UB_j\right)$, the elevation angle is $\varphi_{ab}=\arcsin\left(\frac{h_U}{d_{ab}}\right)$ and the distance between a and b is $d_{ab}=\sqrt{\left(x_b-x_a\right)^2+\left(y_b-y_a\right)^2+{h_U}^2}$; σ is the path-loss exponent; $\mathfrak{A}$ and $\mathfrak{B}$ are constant environment values; and $\mathfrak{K}_l$ is parameters which are contingent on the external environment and carrier frequency, and are expressed as:

$$\mathfrak{K}_l=\mathfrak{D}_l\left(\frac{c}{4\pi f_c}\right)^{-1}, \tag{2}$$

where $l\in\{LoS,NLoS\}$, f_c is the carrier frequency, c is the speed of light, and $\mathfrak{D}_l$ is the excessive path losses of the LoS and NLoS propagation. Assume that all EDs execute the same task of length L (bits) and are classified [6]. Hence, the offloading capacity of A_i and B_j can be written as:

$$C_{\psi}^{off}=\beta_{\psi}L, \tag{3}$$

where $\psi\in\left(A_i,B_j\right)$ and $\beta_{\psi},0\leq\beta_{\psi}\leq 1$ is the offloading ratio. The channel from the $\psi\rightarrow U$ and $\psi\rightarrow E$ are denoted by $g_{\psi U}$ and $g_{\psi E}$, respectively. We assume that the wireless channels between ground EDs and UAV are assumed to experience small-scale quasi-static frequency non-selective fading [15], and that all channel state information (CSI) is perfectly known at the U via channel estimate methods and the system operates under a Rayleigh fading channel with an average channel gain of $\lambda_{\kappa},\kappa\in\left(\psi U,\psi E\right)$ and is affected by the additive white Gaussian noise (AWGN) has a zero mean and N_0 variance. Let $\left|g_{\kappa}\right|^2$ be the channel power gain, thus the cumulative distribution function (CDF) and probability density function (PDF) of $\left|g_{\kappa}\right|^2$ are respectively expressed as:

$$F_{\left|g_{\kappa}\right|^2}\left(x\right)=1-e^{-\frac{x}{\lambda_{\kappa}}}, \tag{4}$$

$$f_{\left|g_{\kappa}\right|^2}\left(x\right)=\frac{1}{\lambda_{\kappa}}e^{-\frac{x}{\lambda_{\kappa}}}. \tag{5}$$

2.2 Communication protocol

This subsection describe the communication protocol of the above system. The protocol's time flowchart, illustrated in Fig 2, can be described as follows.

- In the t^{para} phase: U sends pilot signals to two ED clusters and collects all system connections' CSI in order to estimate SNRs of every transmission

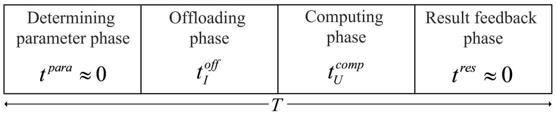

Fig. 2: Time flowchart of the considered UAV NOMA-MEC network.

channels. UAV determines the ED having the greatest SNR for offloading performance, denoted as $\psi^* \in (A^*, B^*)$. Thus, the channel power gains of ψ^* is as [2]:

$$|g_{\psi^*}|^2 = \max_{\substack{\psi \in (A_i, B_j), \\ 1 \leq i \leq N, \\ 1 \leq j \leq M.}} \left\{ |g_\psi|^2 \right\}. \tag{6}$$

Accordingly, the CDF and PDF of $|g_{\psi^*}|^2$ are rewritten as follows, respectively:

$$F_{|g_{\psi^*}|^2}(x) = \sum_{k=0}^{\mathit{\Omega}} \binom{\mathit{\Omega}}{k} (-1)^k e^{-\frac{kx}{\lambda_{\psi^*}}}, \tag{7}$$

$$f_{|g_{\psi^*}|^2}(x) = \sum_{k=1}^{\mathit{\Omega}} \binom{\mathit{\Omega}}{k} \frac{(-1)^{k+1} k}{\lambda_{\psi^*}} e^{-\frac{kx}{\lambda_{\psi^*}}}, \tag{8}$$

where $\mathit{\Omega} \in (N, M)$.

- During the second phase $t_{\psi^*}^{off}$, ψ^* based on uplink NOMA to offload their tasks to U. The following is the received signal at U:

$$y_U^{MEC} = \sqrt{\frac{\rho_{A^*} P}{\mathfrak{L}_{A^*U}}} g_{A^*U} x_A + \sqrt{\frac{\rho_{B^*} P}{\mathfrak{L}_{B^*U}}} g_{B^*U} x_B + n_U, \tag{9}$$

where x_A and x_B are the two best transmitted signal of A^* and B^*; P is the transmit power of EDs; ρ_{A^*} and ρ_{B^*} are the power allocation coefficient, $\rho_{A^*} > \rho_{B^*}, \rho_{A^*} + \rho_{B^*} = 1$; $n_U \sim \mathcal{CN}(0, N_0)$ is AWGN. Here, U assumes that x_B is interference and decodes x_A. Subsequently, in order to decode x_B, U applies SIC to eliminate the previously decoded x_A [3]. Accordingly, the expressions to represent the received signal-to-interference-plus-noise ratios (SINRs) for x_A and x_B detection at U are written as:

$$\gamma_{A^*}^U = \frac{\gamma_{A^*U} |g_{A^*U}|^2}{\gamma_{B^*U} |g_{B^*U}|^2 + 1}, \tag{10}$$

$$\gamma_{B^*}^U = \gamma_{B^*U} |g_{B^*U}|^2, \tag{11}$$

where $\gamma_0 = \frac{P}{N_0}$, $\gamma_{A^*U} = \frac{\rho_{A^*}\gamma_0}{\mathfrak{L}_{A^*U}}$, and $\gamma_{B^*U} = \frac{\rho_{B^*}\gamma_0}{\mathfrak{L}_{B^*U}}$. Similarly, the expression of signal received at E is as follows:

$$y_E = \sqrt{\frac{\rho_{A^*} P}{d_{A^*E}^\sigma}} g_{A^*E} x_A + \sqrt{\frac{\rho_{B^*} P}{d_{B^*E}^\sigma}} g_{B^*E} x_B + n_E, \tag{12}$$

where $n_E \sim \mathcal{CN}\left(0, N_E\right)$ is AWGN at E. We suppose E also applies SIC, similarly, the SINR to detect x_A and x_B at E is given by

$$\gamma_{A^*}^{E} = \frac{\gamma_{A^*E}{\left|g_{A^*E}\right|}^2}{\gamma_{B^*E}{\left|g_{B^*E}\right|}^2 + 1}, \tag{13}$$

$$\gamma_{B^*}^{E} = \gamma_{B^*E}{\left|g_{B^*E}\right|}^2, \tag{14}$$

where $\gamma_E = \frac{P_E}{N_E}$, $\gamma_{A^*E} = \frac{\rho_{A^*}\gamma_E}{d_{A^*E}^{\sigma}}$ and $\gamma_{B^*E} = \frac{\rho_{B^*}\gamma_E}{d_{B^*E}^{\sigma}}$.

- In the third phase, the offloaded tasks is calculated by MEC located at U during t_U^{comp}. The duration required to accomplish the computing processes for the number of task bits at U is as follows:

$$t_U^{comp} = \frac{\left(C_{A^*}^{off} + C_{B^*}^{off}\right)\varsigma}{f_U^{MEC}}, \tag{15}$$

  where ς is the number of CPU cycles needed to complete the calculation for a single input bit and f_U^{MEC} is the MEC operating frequency at U.
- In the fourth phase, U return the processed results to ψ^* during t^{res}. Following [6], t^{para} and t^{res}, are assumed very small compared to $t_{\psi^*}^{off}$, and t_U^{comp}, thus they are neglected.

2.3 Time offloading and secrecy capacity

The instantaneous channel capacity of legitimate $\psi^* \to U$ links is as the following:

$$C_{\psi^*}^{U} = W\log_2\left(1 + \gamma_{\psi^*}^{U}\right), \tag{16}$$

where W is the bandwidth. Thus, the offloading duration from ψ^* to U is formulated by:

$$t_{\psi^*}^{off} = \frac{C_{\psi^*}^{off}}{C_{\psi^*}}. \tag{17}$$

The instantaneous secrecy capacity of wireless communication from ψ^* to U in the presence of a passive eavesdropper is defined as follows [16]:

$$\begin{aligned} C_{\psi^*}^{S} &= \left\lceil C_{\psi^*}^{U} - C_{\psi^*}^{E}\right\rceil^{+} \\ &= \begin{cases} W\log_2\left(\frac{1+\gamma_{\psi^*}^{U}}{1+\gamma_{\psi^*}^{E}}\right), & \gamma_{\psi^*}^{U} > \gamma_{\psi^*}^{E} \\ 0, & \gamma_{\psi^*}^{U} \le \gamma_{\psi^*}^{E} \end{cases}, \end{aligned} \tag{18}$$

where $C_{\psi^*}^{E} = W\log_2\left(1 + \gamma_{\psi^*}^{E}\right)$ is the illegal channel capacity.

3 Performance Analysis

3.1 Secrecy successful computation probability (SSCP)

In this subsection, we presents the secrecy and offloading performance of the system under consideration in terms of SSCP [17], denoted by $\mathcal{S}$. The $\mathcal{S}$ is defined as the probability that all offloading tasks are completed within the maximum permissible system latency T_{th} and the corresponding secrecy capacity is greater than a predefined data rate threshold R_{th}. Thus, the $\mathcal{S}$ of the entire system is calculated as follows:

$$\mathcal{S} = \Pr\left\{ t_{A^*}^{off} \leq T_{th}, t_{B^*}^{off} \leq T_{th}, C_{A^*}^{s} \geq R_{A^*}, C_{B^*}^{s} \geq R_{B^*} \right\}, \tag{19}$$

where $T_{th} = T - t_U^{comp}$, $R_{\psi^*} = \frac{C_{\psi^*}^{off}}{T_{th}}$ [1].

Theorem 1. *The closed-form expression for the SSCP of the entire system for UAV-aided NOMA-MEC under quasi-static Rayleich fading is as follows:*

$$\begin{aligned} \mathcal{S} = \sum_{u=1}^{M}\sum_{k=1}^{N} \binom{M}{u}\binom{N}{k} \frac{(-1)^{u+1}(-1)^{k+1}u}{\lambda_{B^*U}} \Bigg[& \frac{e^{-\varXi_1^{(k,u)}\varDelta_1 - \varXi_2^{(k)}}}{\varXi_1^{(k,u)}} - \frac{e^{-\varXi_3^{(k,u)}\varDelta_1 - \varXi_4^{(k)}}}{\varXi_3^{(k,u)}} \\ & - \frac{\pi^2 k e^{-\varDelta_1}}{4OQ\lambda_{A^*U}\lambda_{B^*E}} \sum_{q=1}^{Q}\sum_{o=1}^{O} \sqrt{\left(1-{\zeta_q}^2\right)\left(1-{\zeta_o}^2\right)} {\omega_o}^{\frac{k}{\lambda_{A^*U}}-1} {\omega_q}^{\frac{u}{\lambda_{B^*U}}-1} \\ & \times \frac{e^{-\varDelta_2^{(\delta_q)} - \varDelta_5^{(\delta_o,\delta_q)}}}{\varDelta_4^{(\delta_o,\delta_q)}} \left(1 - e^{-\varDelta_3^{(\delta_q)}\varDelta_4^{(\delta_o,\delta_q)}}\right) \Bigg], \end{aligned} \tag{20}$$

where $\phi_{A^*} = 2^{\frac{C_{A^*}^{off}}{T_{th}W}} - 1$, $\phi_{B^*} = 2^{\frac{C_{B^*}^{off}}{T_{th}W}} - 1$, $\theta_{A^*} = 2^{\frac{R_{A^*}}{W}}$, $\theta_{B^*} = 2^{\frac{R_{B^*}}{W}}$, $\varDelta_1 = \frac{\phi_{B^*}}{\gamma_{B^*U}}$ *and* $\varXi_1^{(k,u)}$, $\varXi_2^{(k)}$, $\varXi_3^{(k,u)}$, $\varXi_4^{(k)}$, $\varDelta_2^{(\delta_q)}$, $\varDelta_3^{(\delta_q)}$, $\varDelta_4^{(\delta_o,\delta_q)}$, *and* $\varDelta_5^{(\delta_o,\delta_q)}$ *are defined as follows:*

$$\varXi_1^{(k,u)} = \frac{k\phi_{A^*}\gamma_{B^*U}}{\lambda_{A^*U}\gamma_{A^*U}} + \frac{u}{\lambda_{B^*U}}, \tag{21}$$

$$\varXi_2^{(k)} = \frac{k\phi_{A^*}}{\lambda_{A^*U}\gamma_{A^*U}}, \tag{22}$$

$$\varXi_3^{(k,u)} = \frac{\gamma_{B^*U}}{\lambda_{B^*E}\theta_{B^*}\gamma_{A^*E}} + \varXi_1^{(k,u)}, \tag{23}$$

$$\varXi_4^{(k)} = \frac{1-\theta_{B^*}}{\lambda_{B^*E}\theta_{B^*}\gamma_{A^*E}} + \varXi_2^{(k)}, \tag{24}$$

$$\Delta_2^{(\delta_q)} = \frac{\phi_{A^*}\left(\gamma_{B^*U}\delta_q + 1\right)}{\gamma_{A^*U}}, \tag{25}$$

$$\Delta_3^{(\delta_q)} = \frac{\gamma_{B^*U}\delta_q + 1 - \theta_{B^*}}{\theta_{B^*}\gamma_{B^*E}}, \tag{26}$$

$$\Delta_4^{(\delta_o,\delta_q)} = \left(\frac{\gamma_{A^*U}\delta_o}{\gamma_{B^*U}\delta_q + 1} + 1 - \theta_{A^*}\right)\frac{\gamma_{B^*E}}{\lambda_{A^*E}\theta_{A^*}\gamma_{A^*E}} + \frac{1}{\lambda_{B^*E}}, \tag{27}$$

$$\Delta_5^{(\delta_o,\delta_q)} = \left(\frac{\gamma_{A^*U}\delta_o}{\gamma_{B^*U}\delta_q + 1} + 1 - \theta_{A^*}\right)\frac{1}{\lambda_{A^*E}\varphi_{A^*}\gamma_{A^*E}}, \tag{28}$$

where $\zeta_o = \cos\left(\frac{\pi(2o-1)}{2O}\right)$, $\omega_o = \frac{(\zeta_o+1)e^{-\Delta_2^{(\delta_q)}}}{2}$, $\zeta_q = \cos\left(\frac{\pi(2q-1)}{2Q}\right)$, $\omega_q = \frac{(\zeta_q+1)e^{-\Delta_1}}{2}$ *with* O *and* Q *are the complexity versus accuracy trade-off coefficient,* $\delta_q = -\ln(\omega_q)$, $\delta_o = -\ln(\omega_o)$.

Proof. See Appendix A.

3.2 Optimization: problem formulation and solution

To enhance system performance, we focus on enhancing the secrecy and successful computation performance of the entire system by determining the optimal location and altitude of UAV, denoted by (x_U^*, y_U^*, h_U^*). In order to accomplish this, we formulate the SSCP maximization problem and solve it using a PSO-based algorithm.

SSCP maximization problem:

$$\begin{aligned} \text{(P1):}\ & \underset{x_U, y_U, h_U}{\text{maximize}} && \mathcal{S} \\ & \text{subject to} && 0 \leq x_U \leq x_U^{\max}, && \text{(29a)} \\ & && 0 \leq y_U \leq y_U^{\max}, && \text{(29b)} \\ & && 30 \leq h_U \leq h_U^{\max}, && \text{(29c)} \end{aligned}$$

where constraints (29a) and (29b) represent conditions on the UAV's projected location on the ground, constraint (29c) imposes conditions on the altitude of the UAV.

To solve the problem (29) with multiple constraints, we propose the PSO algorithm [2], a stochastic, population-based algorithm modeled on SI that can tackle complex optimization problems. **Algorithm 1** presents the overall SSCP maximization based on PSO (SSCPMax-PSO) algorithm used for our proposed system model. The algorithm begins by randomly initializing particles $i = [1, \mathcal{N}]$. Each particle i has a current position $\mathcal{X}_i = (x_U, y_U, h_U)$, a current velocity $\mathcal{V}_i$, a personal best position $\mathcal{X}_i^*$ that corresponds to the position where the particle had the highest value of the SSCP objective function (for the maximization problem), and a global best position $\mathcal{G}_b$ that corresponds to the best position among all personal best positions. SSCPMax-PSO's main loop is iterated $\mathcal{I}$ times to find the particle with the best $\mathcal{X}_i^*$ and $\mathcal{G}_b$. Each particle's velocity $\mathcal{V}_i$, position $\mathcal{X}_i$, and optimal values $\mathcal{X}_i^*$ and $\mathcal{G}_b$ are updated during each iteration.

Algorithm 1 SSCPMax-PSO

```
Require: $\mathcal{N}$, $\mathcal{I}$, $\mathcal{S}$, $\varpi$, $\chi$, $\epsilon_1$, $\epsilon_2$, and constraint conditions
Ensure: $x_U^*$, $y_U^*$, $h_U^*$

function SSCP_MAX
    Set parameters of PSO: $\mathcal{N}$; $\mathcal{I}$; $\varpi$; $\chi$; $\epsilon_1$; $\epsilon_2$;
    Initialize global best: $\mathcal{G}_b = \infty$;
    Initialize population members:
    for $i = 1 : \mathcal{N}$ do
        Generate random solution: $\mathcal{X}_i(x_U, y_U, h_U)$;
        Initialize velocity: $\mathcal{V}_i = 0$;
        Evaluation of particle $i$: $\mathcal{C}_i = 1 - \mathcal{S}\left(\mathcal{X}_i\right)$;
        Update the personal best: $\mathcal{X}_i^* = \mathcal{X}_i; \mathcal{C}_i^* = \mathcal{C}_i$;
        Update global best:
        if $\mathcal{C}_i^* < \mathcal{G}_b$ then
            $\mathcal{G}_b = \mathcal{C}_i^*$;
        end if
    end for
     Main loop of SSCP-PSO algorithm
    Array to hold best cost value in each iteration: $\mathcal{B}$ =zeros($\mathcal{I}$, 1);
    for $j = 1 : \mathcal{I}$ do
        for $i = 1 : \mathcal{N}$ do
            Update velocity: $\mathcal{V}_i = \chi \mathcal{V}_{i-1} + \epsilon_1 r_1 \left(\mathcal{X}_{i-1}^* - \mathcal{X}_{i-1}\right)$
                                    $+\epsilon_2 r_2 \left(\mathcal{X}_{\mathcal{G}_b, i-1} - \mathcal{X}_{i-1}\right)$;
            Update position: $\mathcal{X}_i = \mathcal{X}_{i-1} + \mathcal{V}_i$;
            Evaluation of particle $i$: $\mathcal{C}_i = 1 - \mathcal{S}\left(\mathcal{X}_i\right)$;
            Update personal best:
            if $\mathcal{C}_i < \mathcal{C}_i^*$ then
                $\mathcal{X}_i^* = \mathcal{X}_i$;
                $\mathcal{C}_i^* = \mathcal{C}_i$;
                Update global best (find $x_U^*$, $y_U^*$ and $h_U^*$ of UAV):
                if $\mathcal{C}_i^* < \mathcal{G}_b$ then
                    $\mathcal{G}_b = \mathcal{C}_i^*$;
                end if
            end if
        end for
        Store the best cost value: $\mathcal{B}(j) = \mathcal{G}_b$
    end for
    return $\mathcal{B}$;
end function
```

Table 1: Simulation parameter.

Parameter	**Value**	**Parameter**	**Value**	**Parameter**	**Value**
(x_A, y_A)	$(40, 0)$ (m)	$\mathfrak{A}$	0.1581	P	$(0, 20)$ (dB)
(x_B, y_B)	$(0, 40)$ (m)	$\mathfrak{B}$	9.6177	T	0.5 (s)
(x_E, y_E)	$(75, 75)$ (m)	$\mathfrak{O}_{LoS}$	1	ρ	0.75
x_U	$(0, 50)$ (m)	$\mathfrak{O}_{NLoS}$	20	σ	2
y_U	$(0, 50)$ (m)	c	3.10^8	W	10^8
h_U	$(20, 100)$ (m)	f_c	10^7	$\beta_A = \beta_B$	0.5
L	10^4	f_U^{MEC}	10^8	$\mathcal{I}$	10^2
$O = Q$	10^2	ς	10^2	$\mathcal{N}$	100

4 Numerical result

This section provided the numerical results that were utilized to verify the analytical expression of the SSCP described in Section 3 for the UAV-aided NOMA-MEC in IoT network. Specifically, we consider the following system parameters in all simulations, shown in Table 1 [2,14].

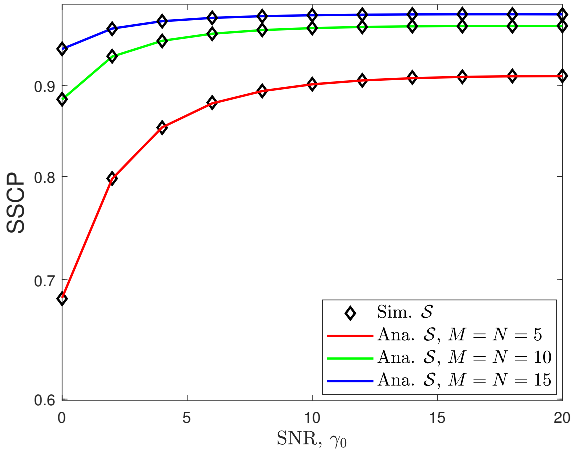

Fig. 3: Impact of average transmit SNR, (γ_0) on SSCP of the entire system with different number of ED in two clusters.

The impact of the average SNR γ_0 and the number of ED clusters on the SSCP of the entire system is depicted in Fig. 3. We can observe that the Monte Carlo simulation and our analysis have a powerful match, confirming the accuracy of our proposed model. Moreover, when the number of devices in the two clusters is increased, SSCP also increases. This is due to the fact that as the number of devices grows, the UAV has more options to select the best ED in two clusters. Furthermore, increasing the transmit power of the device improves the system's security offload performance. Because, as the transmit power increases, the device has more power to communicate with the UAV.

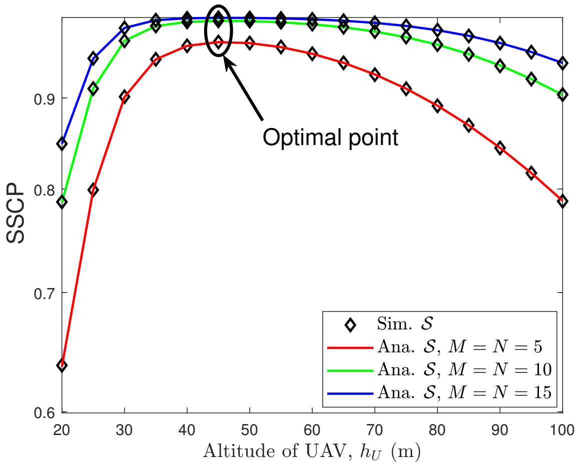

Fig. 4: Impact of altitude of UAV, (h_U) on SSCP of the entire system with different number of ED in two clusters.

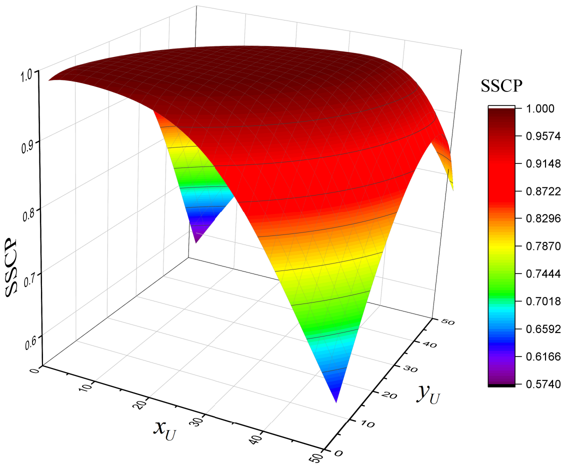

Fig. 5: Impact of the location of UAV, (x_U, y_U) on SSCP of the entire system.

Fig. 4 depicts of the altitude of UAV, h_U and the number of ED clusters, N, M on the SSCP of the entire system. we can also see that there will be an altitude of the UAV to maximize performance; this can explain why, when the altitude of the UAV is low, the probability of encountering NLoS is greater than the probability of encountering LoS due to urban obstacles. The increased UAV altitude improves performance because the probability of confronting an LoS between the UAV and the ED is greater than the probability of encountering an NLoS. Nonetheless, the greater the altitude, the greater the communication distance between the UAV and the ED, which increases the pass loss of the UAV-ED links and consequently decreases the performance. So there will be an altitude that maximizes the efficacy of secrecy offloading.

In addition to the problem of the UAV's altitude, we must also consider the UAV's location so that the communication between it and the ED is better. As shown in Fig. 5, this is the 3D result depicting the SSCP value domain as a result of the simultaneous effects of x_U and y_U. We have observed that there exists an x_U^* and y_U^* position that optimizes the performance of the system. This is understandable; the UAV will select the optimal location to communicate with the ED of the two clusters. This is regarded as an outstanding characteristic of UAV

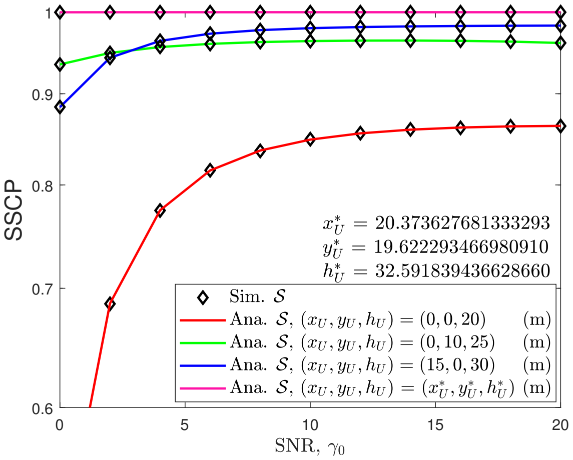

Fig. 6: Impact of the location and altitude of UAV, (x_U^*, y_U^*, h_U^*) on SSCP of the entire system.

Fig. 6 depicts the impact of the location and altitude of UAV, (x_U^*, y_U^*, h_U^*) on SSCP of the entire system. In this result, we replace the optimal values found from solving the proposed optimization problem above (**Algorithm 1**). We compare SSCP(x_U^*, y_U^*, h_U^*) with SSCPs with fixed (x_U, y_U, h_U) values. The results show that with the application of SSCPMax-PSO algorithm to give the optimal values, the secret offload performance is the best compared to our self-fixing for the UAV.

5 Conclusion

In this paper, we investigated the secrecy offloading performance of an UAV-aided NOMA-MEC in IoT over Rayleigh fading channel. We propose a fourth-phase system operating protocol based on UAV-ED selection, focusing NOMA-MEC techniques to increase the secrecy offloading performance. To assess the system performance, we obtain closed-form expressions of SSCP of the entire system. In addition, we proposed an PSO based algorithm to determine the location and altitude of a UAV to maximize the SSCP. Numerical results are presented to validate the proposed system's secrecy offloading performance.

A Proof of Theorem 1

By substituting (3), (10), (11), (13), (14), (15), (16), (17), (18) into (19), we can rewrite the $\mathcal{S}$ of system as

$$\begin{aligned}\mathcal{S} = \Pr\Bigg\{ & X > \mathit{\Delta}_2^{(Y)}, Y > \mathit{\Delta}_1, P < \mathit{\Delta}_3^{(Y)}\ , \\ & \qquad Z < \left(\frac{\gamma_{A^*U}X}{\gamma_{B^*U}Y+1} + 1 - \theta_{A^*}\right)\frac{\gamma_{B^*E}P+1}{\theta_{A^*}\gamma_{A^*E}}\Bigg\}, \\ = & \int\limits_{\mathit{\Delta}_1}^{\infty}\int\limits_{\mathit{\Delta}_2^{(Y)}}^{\infty}\int\limits_{0}^{\mathit{\Delta}_3^{(Y)}} F_Z\left[\left(\frac{\gamma_{A^*U}X}{\gamma_{B^*U}Y+1} + 1 - \theta_{A^*}\right)\frac{\gamma_{B^*E}P+1}{\theta_{A^*}\gamma_{A^*E}}\right] \\ & \qquad\qquad \times f_P\left(P\right) f_X\left(X\right) f_Y\left(Y\right) dPdXdY, \end{aligned} \tag{30}$$

where $X = \left|g_{A^*U}\right|^2$, $Y = \left|g_{B^*U}\right|^2$, $Z = \left|g_{A^*E}\right|^2$, $P = \left|g_{B^*E}\right|^2$, $\mathit{\Delta}_1 = \frac{\phi_{B^*}}{\gamma_{B^*U}}$, $\mathit{\Delta}_2^{(Y)} = \frac{\phi_{A^*}(\gamma_{B^*U}Y+1)}{\gamma_{A^*U}}$, $\mathit{\Delta}_3^{(Y)} = \frac{\gamma_{B^*U}Y+1-\theta_{B^*}}{\theta_{B^*}\gamma_{B^*E}}$. There are three integrals here, so we do the integration one by one. First, we solve the 1st integral, denoted by I_1. By combining the CDF in (4) and the PDF in (5) into I_1, we can rewrite as follow:

$$\begin{aligned} I_1 = & \int\limits_0^{\mathit{\Delta}_3^{(Y)}} \left(1 - e^{-\left(\frac{\gamma_{A^*U}X}{\gamma_{B^*U}Y+1}+1-\theta_{A^*}\right)\frac{(\gamma_{B^*E}P+1)}{\lambda_{A^*E}\theta_{A^*}\gamma_{A^*E}}}\right)\frac{1}{\lambda_{B^*E}}e^{-\frac{P}{\lambda_{B^*E}}}dP \\ = & \frac{1}{\lambda_{B^*E}}\left(\int\limits_0^{\mathit{\Delta}_3^{(Y)}} e^{-\frac{P}{\lambda_Q}}dP - e^{-\mathit{\Delta}_5^{(X,Y)}}\int\limits_0^{\mathit{\Delta}_3^{(Y)}} e^{-\mathit{\Delta}_4^{(X,Y)}P}dP\right), \end{aligned} \tag{31}$$

where $\Delta_4^{(X,Y)} = \left(\frac{\gamma_{A^*U}X}{\gamma_{B^*U}Y+1} + 1 - \theta_{A^*}\right)\frac{\gamma_{B^*E}}{\lambda_{A^*E}\theta_{A^*}\gamma_{A^*E}} + \frac{1}{\lambda_{B^*E}}$ and $\Delta_5^{(X,Y)} = \left(\frac{\gamma_{A^*U}X}{\gamma_{B^*U}Y+1} + 1 - \theta_{A^*}\right)\frac{1}{\lambda_{A^*E}\theta_{A^*}\gamma_{A^*E}}$. The integrals in (31) are solved by applying the Eq. (3.351.1^{8}) in [18] shown in (32).

$$I_1 = 1 - e^{-\frac{\Delta_3^{(Y)}}{\lambda_{B^*E}}} - \frac{e^{-\Delta_5^{(X,Y)}}}{\lambda_{B^*E}\Delta_4^{(X,Y)}}\left(1 - e^{-\Delta_3^{(Y)}\Delta_4^{(X,Y)}}\right). \tag{32}$$

Next, we substitute I_1 in (32) and the PDF in (8) into the 2nd integral, denoted by I_2, which can be expressed as follows:

$$\begin{aligned} I_2 = \sum_{k=1}^{N}\binom{N}{k}\frac{(-1)^{k+1}k}{\lambda_{A^*U}} \Bigg[& \underbrace{\int_{\Delta_2^{(Y)}}^{\infty} e^{-\frac{kX}{\lambda_{A^*U}}}dX - \int_{\Delta_2^{(Y)}}^{\infty} e^{-\frac{\Delta_3^{(Y)}}{\lambda_{B^*E}}-\frac{kX}{\lambda_{A^*U}}}dX}_{I_{21}} \\ & \underbrace{- \int_{\Delta_2^{(Y)}}^{\infty} \frac{e^{-\Delta_5^{(X,Y)}-\frac{kX}{\lambda_{A^*U}}}}{\lambda_{B^*E}\Delta_4^{(X,Y)}}\left(1 - e^{-\Delta_3^{(Y)}\Delta_4^{(X,Y)}}\right)dX}_{I_{22}}\Bigg], \end{aligned} \tag{33}$$

From (33), for I_{21}, we solve the integrals by Eq. (3.351.1^{11}) in [18], shown in (34). For I_{22}, let $v = e^{-X}$ and $X = -\ln(v)$, then I_{22} solved by applying the Gaussian-Chebyshev quadrature method [19], shown in (34).

$$\begin{aligned} I_{21} &= \int_{\Delta_2^{(Y)}}^{\infty} e^{-\frac{kX}{\lambda_{A^*U}}}dX - \int_{\Delta_2^{(Y)}}^{\infty} e^{-\frac{\Delta_3^{(Y)}}{\lambda_{B^*E}}-\frac{kX}{\lambda_{A^*U}}}dX \\ &= \frac{\lambda_{A^*U}}{k}e^{-\frac{k\Delta_2^{(Y)}}{\lambda_{A^*U}}} - \frac{\lambda_{A^*U}}{k}e^{-\frac{\Delta_3^{(Y)}}{\lambda_{B^*E}}-\frac{k\Delta_2^{(Y)}}{\lambda_{A^*U}}}, \end{aligned} \tag{34}$$

$$\begin{aligned} I_{22} &= \int_{0}^{e^{-\Delta_2^{(Y)}}} \frac{v^{\frac{k}{\lambda_X}-1}e^{-\Delta_5^{(-\ln(v),Y)}}}{\lambda_{B^*E}\Delta_4^{(-\ln(v),Y)}}\left(1 - e^{-\Delta_3^{(Y)}\Delta_4^{(-\ln(v),Y)}}\right)dv \\ &= \frac{\pi e^{-\Delta_2^{(Y)}}}{2O}\sum_{o=1}^{O}\sqrt{1-{\zeta_o}^2}\frac{{\omega_o}^{\frac{k}{\lambda_X}-1}e^{-\Delta_5^{(\delta_o,Y)}}}{\lambda_{B^*E}\Delta_4^{(\delta_o,Y)}}\left(1 - e^{-\Delta_3^{(Y)}\Delta_4^{(\delta_o,Y)}}\right), \end{aligned} \tag{35}$$

where $\zeta_o = \cos\left(\frac{\pi(2o-1)}{2O}\right)$, $\omega_o = \frac{(\zeta_o+1)e^{-\Delta_2^{(Y)}}}{2}$, $\delta_o = -\ln(\omega_o)$, and O is the complexity versus accuracy trade-off coefficient. Combining (34) and (35), I_2 is rewritten as

$$\begin{aligned} I_2 = \sum_{k=1}^{N} \binom{N}{k} (-1)^{k+1} \Bigg[& e^{-\frac{k\Delta_2^{(Y)}}{\lambda_{A^*U}}} - e^{-\frac{\Delta_3^{(Y)}}{\lambda_{B^*E}} - \frac{k\Delta_2^{(Y)}}{\lambda_{A^*U}}} \\ & - \frac{\pi k e^{-\Delta_2^{(Y)}}}{2O\lambda_{A^*U}\lambda_{B^*E}} \sum_{o=1}^{O} \sqrt{1-{\zeta_o}^2} \frac{{\omega_o}^{\frac{k}{\lambda_{A^*U}}-1} e^{-\Delta_5^{(\delta_o,Y)}}}{\Delta_4^{(\delta_o,Y)}} \left(1 - e^{-\Delta_3^{(Y)}\Delta_4^{(\delta_o,Y)}}\right) \Bigg]. \end{aligned} \tag{36}$$

Finally, we combine I_2 in (36) and the PDF in (8) into the last integral in (30), then $\mathcal{S}$ is expressed as:

$$\begin{aligned} \mathcal{S} = & \sum_{u=1}^{M} \binom{M}{u} \frac{(-1)^{u+1}u}{\lambda_{B^*U}} \sum_{k=1}^{N} \binom{N}{k} (-1)^{k+1} \\ & \times \Bigg[\underbrace{e^{-\Xi_2^{(k)}} \int_{\Delta_1}^{\infty} e^{-\Xi_1^{(k,u)}Y} dY - e^{-\Xi_4^{(k)}} \int_{\Delta_1}^{\infty} e^{-\Xi_3^{(k,u)}Y} dY}_{I_{31}} - \frac{\pi k}{2O\lambda_{A^*U}\lambda_{B^*E}} \\ & \times \sum_{o=1}^{O} \sqrt{1-{\zeta_o}^2} \underbrace{\int_{\Delta_1}^{\infty} e^{-\Delta_2^{(Y)}} \frac{{\omega_o}^{\frac{k}{\lambda_{A^*U}}-1} e^{-\Delta_5^{(\delta_o,Y)} - \frac{uY}{\lambda_{B^*U}}}}{\Delta_4^{(\delta_o,Y)}} \left(1 - e^{-\Delta_3^{(Y)}\Delta_4^{(\delta_o,Y)}}\right) dY}_{I_{32}} \Bigg], \end{aligned} \tag{37}$$

where $\Xi_1^{(k,u)} = \frac{k\phi_{A^*}\gamma_{B^*U}}{\lambda_{A^*U}\gamma_{A^*U}} + \frac{u}{\lambda_{B^*U}}$, $\Xi_2^{(k)} = \frac{k\phi_{A^*}}{\lambda_{A^*U}\gamma_{A^*U}}$, $\Xi_3^{(k,u)} = \frac{\gamma_{B^*U}}{\lambda_{B^*E}\theta_{B^*}\gamma_{A^*E}} + \Xi_1^{(k,u)}$, and $\Xi_4^{(k)} = \frac{1-\theta_{B^*}}{\lambda_{B^*E}\theta_{B^*}\gamma_{A^*E}} + \Xi_2^{(k)}$. Similar to the integral solution of I_2. I_{31} and I_{32} are expressed as follows:

$$I_{31} = \frac{e^{-\Xi_1\Delta_1 - \Xi_2}}{\Xi_1} - \frac{e^{-\Xi_3\Delta_1 - \Xi_4}}{\Xi_3}, \tag{38}$$

$$\begin{aligned} I_{32} = & \frac{\pi^2 k e^{-\Delta_1}}{4OQ\lambda_{A^*U}\lambda_{B^*E}} \sum_{q=1}^{Q} \sum_{o=1}^{O} \sqrt{1-{\zeta_q}^2} \sqrt{1-{\zeta_o}^2} \\ & \times {\omega_o}^{\frac{k}{\lambda_{A^*U}}-1} {\omega_q}^{\frac{u}{\lambda_{B^*U}}-1} e^{-\Delta_2^{(\delta_q)} - \Delta_5^{(\delta_o,\delta_q)}} \frac{1 - e^{-\Delta_3^{(\delta_q)}\Delta_4^{(\delta_o,\delta_q)}}}{\Delta_4^{(\delta_o,\delta_q)}}, \end{aligned} \tag{39}$$

where $\zeta_q = \cos\left(\frac{\pi(2q-1)}{2Q}\right)$, $\omega_q = \frac{(\zeta_q+1)e^{-\Delta_1}}{2}$, and $\delta_q = -\ln(\omega_q)$ with Q is the complexity versus accuracy trade-off coefficient. By substituting (38) and (39) into (37), the closed-form expression for the SSCP of the entire system is obtained as given in Theorem 1.

References

1. B. Li, W. Wu, W. Zhao, and H. Zhang, "Security enhancement with a hybrid cooperative NOMA scheme for MEC system," *IEEE Trans. Veh. Technol.*, vol. 70, no. 3, pp. 2635–2648, Mar. 2021.
2. A.-N. Nguyen, D.-B. Ha, V. N. Vo, V.-T. Truong, D.-T. Do, and C. So-In, "Performance analysis and optimization for iot mobile edge computing networks with RF energy harvesting and UAV relaying," *IEEE Access*, vol. 10, pp. 21 526–21 540, Feb. 2022.
3. A.-N. Nguyen, V. N. Vo, C. So-In, and D.-B. Ha, "System performance analysis for an energy harvesting iot system using a DF/AF UAV-enabled relay with downlink NOMA under nakagami-m fading," *Sensors*, vol. 21, no. 1, Jan. 2021.
4. Y. Xu, T. Zhang, J. Loo, D. Yang, and L. Xiao, "Completion time minimization for UAV-assisted mobile-edge computing systems," *IEEE Trans. Veh. Technol.*, vol. 70, no. 11, pp. 12 253–12 259, Nov. 2021.
5. Z. Ding, P. Fan, and H. V. Poor, "Impact of non-orthogonal multiple access on the offloading of mobile edge computing," *IEEE Trans. Commun.*, vol. 67, no. 1, pp. 375–390, Jan. 2019.
6. V.-T. Truong, V. N. Vo, D.-B. Ha, and C. So-In, "On the system performance of mobile edge computing in an uplink NOMA WSN with a multiantenna access point over nakagami-m fading," *IEEE/CAA J. Autom. Sinica*, vol. 9, no. 4, pp. 668–685, Apr. 2022.
7. Y. Guo, C. You, C. Yin, and R. Zhang, "UAV trajectory and communication codesign: Flexible path discretization and path compression," *IEEE J. Sel. Areas Commun.*, vol. 39, no. 11, pp. 3506–3523, Nov. 2021.
8. D. Liu, Y. Xu, J. Wang, J. Chen, K. Yao, Q. Wu, and A. Anpalagan, "Opportunistic UAV utilization in wireless networks: Motivations, applications, and challenges," *IEEE Commun. Mag.*, vol. 58, no. 5, pp. 62–68, May 2020.
9. H. Peng and X. Shen, "Multi-agent reinforcement learning based resource management in MEC- and UAV-assisted vehicular networks," *IEEE J. Sel. Areas Commun.*, vol. 39, no. 1, pp. 131–141, Jan. 2021.
10. A.-N. Nguyen, V. N. Vo, C. So-In, D.-B. Ha, and V.-T. Truong, "Performance analysis in UAV-enabled relay with NOMA under nakagami-m fading considering adaptive power splitting," in *Proc. Int. Joint Conf. Comput Sci. Software Eng.*, Jul. 2021, pp. 1–6.
11. X. Zhou, M. R. McKay, B. Maham, and A. Hjørungnes, "Rethinking the secrecy outage formulation: A secure transmission design perspective," *IEEE Commun. Lett.*, vol. 15, no. 3, pp. 302–304, Mar. 2011.
12. S. Han, X. Xu, S. Fang, Y. Sun, Y. Cao, X. Tao, and P. Zhang, "Energy efficient secure computation offloading in noma-based mmtc networks for iot," *IEEE Internet Things J.*, vol. 6, no. 3, pp. 5674–5690, Jun. 2019.
13. W. Wu, F. Zhou, R. Q. Hu, and B. Wang, "Energy-efficient resource allocation for secure noma-enabled mobile edge computing networks," *IEEE Trans. Commun.*, vol. 68, no. 1, pp. 493–505, Jan. 2020.
14. A.-N. Nguyen, D.-B. Ha, V.-T. Truong, C. So-In, P. Aimtongkham, C. Sakunrasrisuay, and C. Punriboon, "On secrecy analysis of uav-enabled relaying noma systems with rf energy harvesting," in *Proc. Industrial Networks and Intelligent Systems*, Jun. 2022, pp. 267–281.
15. M. Monemi, H. Tabassum, and R. Zahedi, "On the performance of non-orthogonal multiple access (noma): Terrestrial vs. aerial networks," in *Proc. IEEE Eighth Int. Conf. Communi. Netw. (ComNet)*, Oct. 2020, pp. 1–8.

16. A.-N. Nguyen, V. Nhan Vo, C. So-In, D.-B. Ha, S. Sanguanpong, and Z. A. Baig, “On secure wireless sensor networks with cooperative energy harvesting relaying,” *IEEE Access*, vol. 7, pp. 139 212–139 225, Sep. 2019.
17. V.-T. Truong and D.-B. Ha, “A novel secrecy offloading in NOMA heterogeneous mobile edge computing network,” in *Proc. Advanced Engineering – Theory and Applications*, Dec. 2022, pp. 468–477.
18. I. Gradshteyn and I. Ryzhik, *Table of Integrals, Series, and Products*, A. Jeffrey and D. Zwillinger, Eds. USA: Academic Press, 2014.
19. K. L. Judd, “Quadrature methods presented at university of chicago’s initiative for computational economics,” 2012.